Decadal Prediction in the Pacific Region

GERALD A. MEEHL AND AIXUE HU

National Center for Atmospheric Research, Boulder, Colorado*

CLAUDIA TEBALDI+

National Center for Atmospheric Research, Boulder, Colorado, and Climate Central, Princeton, New Jersey*

(Manuscript received 17 June 2009, in final form 14 January 2010)

ABSTRACT

A ''perfect model'' configuration with a global coupled climate model 30-member ensemble is used to address decadal prediction of Pacific SSTs. All model data are low-pass filtered to focus on the low-frequency decadal component. The first three EOFs in the twentieth-century simulation, representing nearly 80% of the total variance, are used as the basis for early twenty-first-century predictions. The first two EOFs represent the forced trend and the interdecadal Pacific oscillation (IPO), respectively, as noted in previous studies, and the third has elements of both trend and IPO patterns. The perfect model reference simulation, the target for the prediction, is taken as the experiment that ran continuously from the twentieth to twenty-first century using anthropogenic and natural forcings for the twentieth century and the A1B scenario for the twenty-first century. The other 29 members use a perturbation in the atmosphere at year 2000 and are run until 2061. Since the IPO has been recognized as a dominant contributor to decadal variability in the Pacific, information late in the twentieth century and early in the twenty-first century is used to select a subset of ensemble members that are more skillful in tracking the time evolution of the IPO (EOF2) in relation to a notional start date of 2010. Predictions for the 19-yr period centered on the year 2020 use that subset of ensemble members to construct Pacific SST patterns based on the predicted evolution of the first three EOFs. Compared to the perfect model reference simulation, the predictions show some skill for Pacific SST predictions with anomaly pattern correlations greater than +0.5. An application of the Pacific SST prediction is made to precipitation over North America and Australia. Even though there are additional far-field influences on Pacific SSTs and North American and Australian precipitation involving the Atlantic multidecadal oscillation (AMO) in the Atlantic, and Indian Ocean and South Asian monsoon variability, there is qualitative skill for the pattern of predicted precipitation over North America and Australia using predicted Pacific SSTs. This exercise shows that, in the presence of a large forced trend like that in the large ensemble, much of Pacific region decadal predictability about 20 years into the future arises from increasing greenhouse gases.

1. Introduction

The new field of decadal prediction focuses on the ''decadal'' (defined as 10 to 30 years in the future) time scale that is of interest to policymakers and stakeholders (Meehl et al. 2009a; Hurrell et al. 2009). There have been several attempts at decadal prediction using initialized global coupled climate models, though these predictions so far have been for 10 years in the future (Smith et al. 2007; Keenlyside et al. 2008; Pohlmann et al. 2009). Recently, decadal hindcasts for the Pacific region have been attempted (Mochizuki et al. 2010).

Both the externally forced response (e.g., from increasing greenhouse gases) and internal variability [e.g., from the interdecadal Pacific oscillation (IPO), the Pacific decadal oscillation (PDO) is the North Pacific component of the basinwide IPO—both have similar patterns] are important sources of potential predictability for Pacific SSTs (Meehl et al. 2009a). Internally generated variability that could be predictable presumes that there are distinct physical mechanisms producing that variability, such as for

* The National Center for Atmospheric Research is sponsored by the National Science Foundation.

+ Current affiliation: Climate Central, Princeton, New Jersey, and University of British Columbia, Vancouver, British Columbia, Canada.

Corresponding author address: Gerald A. Meehl, NCAR, P.O. Box 3000, Boulder CO 80307.
E-mail: meehl@ncar.ucar.edu

DOI: 10.1175/2010JCLI3296.1

the IPO (Meehl and Hu 2006). At a regional level their relative importance varies significantly, with the forced response largest over parts of the tropical oceans and the internal variability contribution greater over the middle- and high-latitude oceans (Boer 2010). In spite of the considerable signal-to-noise issues for shorter-term decadal predictions, there are indications that over the next several decades a detectable predicted response could emerge above the noise (Karoly and Wu 2005). Teng and Branstator (2010) analyzed the large ensemble used in the present paper to show that subsurface heat content anomalies in the North Pacific and North Atlantic are more predictable than surface temperatures, with potential predictability in parts of those regions out to about a decade. Since the predictable component of climate anomalies on decadal time scales in any location is typically modest compared to the unpredictable component, it is important that these types of experiments, including perfect model studies, are performed to begin to quantify estimates of skill.

The so-called ''perfect model'' technique has been used to obtain estimates of predictability assuming the initial state and time evolution of the climate system were known exactly in the form of a reference simulation that perturbed ensemble members would try to predict. Such studies, as well as initialized predictions (e.g., Kirtman and Min 2009), have been used for ENSO predictions to demonstrate that, for predictions 8 months in advance, multimodel correlation coefficients for Niño-3.4 are approximately 0.75, reducing to 0.6 at 10 months and 0.5 at 12 months (Kirtman et al. 2002). However, Tang et al. (2008) have shown that ENSO predictability varies on decadal time scales, thus indicating the greater challenge of longer-term predictions initialized from different climate base states.

It is generally believed that decadal predictions could gain skill from three sources (Meehl et al. 2009a). The first is climate change commitment (e.g., Meehl et al. 2005), whereby the climate system will continue to respond for the next several decades due to forcing already in the system. The second is changes in external forcing, such as increases in greenhouse gases (GHGs) (Lee et al. 2006), that are likely to continue at close to current rates for the next several decades no matter what forcing scenario is followed (Meehl et al. 2007). And the third is the time evolution of regional decadal mechanisms [e.g., the IPO in the Pacific (Power et al. 1999) or tropical–midlatitude interactions in that region (Deser et al. 2004)] that could evolve predictably over perhaps the next decade or two if captured accurately in the initial state. Thus, decadal predictions lie at the confluence of skill from climate change commitment, an initialized climate state (that is currently applied for ENSO forecasts), and the longer-term forced response (Hawkins and Sutton 2009). Exactly where this transition occurs (from initialized skill to forced skill) is not well known. The studies mentioned above that have been performed for decadal prediction have mainly tried to exploit prediction skill from the initial state over the next decade.

Therefore, the purpose of this paper is to perform decadal predictions for Pacific SSTs in relation to a notional year of 2010 for the 19-yr period centered on 2020. Predictions farther in the future will also be discussed although, in relation to 2010 for simulations that start in 2000, a deterministic IPO evolution will likely be near the limit of its contribution at 2020 when the forced response could be expected to become more dominant. A perfect model technique will be used with a 30-member ensemble of twenty-first-century simulations from a global coupled climate model, the Community Climate System Model version 3 (CCSM3). Since the IPO and Pacific SSTs have been shown to influence North American and Australian precipitation, an application will be performed to reconstruct future precipitation patterns in those regions using the SST information from the Pacific.

An implicit assumption in this paper is that far-field influences on Pacific SSTs (and also in part North American and Australian precipitation) such as the Atlantic multidecadal oscillation (AMO) (e.g., Folland et al. 1999; Enfield et al. 2001; Knight et al. 2005; Parker et al. 2007) and Indian Ocean SSTs and South Asian monsoon variability (e.g., Arblaster et al. 2002; Meehl and Hu 2006) are accounted for in the model's simulation of Pacific SSTs. The AMO in the model resembles the pattern of SSTs in the North Atlantic documented by Schubert et al. (2009). Although Atlantic SST variability likely contributes not only to Pacific SST variability (e.g., Timmermann et al. 2007) but also, for example, to North American precipitation variability (Sutton and Hodson 2005; Schubert et al. 2009; the latter indicate a more dominant influence of Pacific SSTs), our focus here is on Pacific region SSTs that likely include those far-field influences. Thus the present study includes a particular emphasis on the IPO, which has been identified as a pattern that is notable for decadal variability in the Pacific (Power et al. 1999; Meehl and Hu 2006). Although the objective of this paper is to predict Pacific SSTs, we will apply those predictions to derive related patterns of precipitation over North America and Australia, mindful that the Atlantic SSTs could also have a significant direct influence over precipitation, particularly in North America (e.g., Schubert et al. 2009). We will show that such a regionally based methodology does produce predictive skill, although a parallel exercise using only Atlantic SSTs for North American precipitation would be another interesting way to approach the problem. Ultimately,

prediction of global SSTs and associated regional precipitation patterns may be a desirable option, though our results suggest that a regional approach could produce some skill for regional predictions.

Section 2 describes the model and the large ensemble, and section 3 outlines the experimental design and decadal prediction methodology. Section 4 will show the results of the decadal predictions in terms of Pacific SSTs, section 5 applies those results to North American and Australian precipitation for a time period centered on the year 2020, and section 6 contains the conclusions.

2. Model description

The Community Climate System Model version 3 (CCSM3) twentieth- and twenty-first-century simulations analyzed here are from the T42 version of CCSM3 with actively coupled ocean, land, and sea ice components (Collins et al. 2006). Grid points in the atmosphere are spaced roughly every 2.8° latitude and longitude, and there are 26 levels in the vertical. The ocean is a version of the Parallel Ocean Program (POP) with a nominal latitude–longitude resolution of 1° (down to ½° in the equatorial tropics) and 40 levels in the vertical. No flux adjustments are used in the CCSM3, and the equilibrium climate sensitivity is 2.7°C with a transient climate response of 1.5°C (Meehl et al. 2006).

The reference simulation or perfect model uses a single simulation of twentieth-century climate (forced by a combination of anthropogenic and natural forcings) that continued without perturbations to the twenty-first century following the A1B scenario (Meehl et al. 2006). Then 29 additional ensemble members were generated for the period 2000 to 2061. The perturbations for the ensemble members involved starting the atmosphere from different days around 1 January 2000, with the other components of the climate system (land, ocean, and sea ice) having the same initial state in each of the ensemble members [see Teng and Branstator (2010), for more details].

This should be considered a conservative method of perturbing the initial state since presumably even greater interensemble spread would occur if the ocean and sea ice were also perturbed. But, as noted by Xie et al. (2010) and Teng and Branstator (2010) and also shown below, there is considerable divergence among ensemble members that results from just perturbing the atmosphere in the coupled model.

3. Experimental design and decadal prediction methodology

Since previous work has shown that low-frequency SST patterns in the Pacific region are likely to be a combination of inherent (internally generated) and externally forced response (Meehl et al. 2009a), the analyses here will attempt to quantify contributions from both of those sources to predictions over the next several decades. The interdecadal Pacific oscillation (the regional manifestation of the IPO in the North Pacific is the Pacific decadal oscillation) has been identified as a dominant contributor to low frequency variability in the Pacific (Power et al. 1999; Meehl and Hu 2006; Meehl et al. 2009b). Therefore, regional predictive skill, over and above that from commitment and external forcing, may be realized if the time evolution of the IPO could be predicted. However, the low frequency nature of the IPO dictates that decadal predictions should be averaged over some future time period. Here we low-pass filter all model data such that a prediction for the year 2020 actually represents an outlook for the 19 years centered on 2020. Narrowing this filter to shorter time periods could also be done, but we use the 19-yr filter as a broad starting point that could be followed in subsequent work by different filtering.

We assume the notional present-day start date for the predictions to be 2010. However, the ensembles branched from the year 2000, so, due to the low-pass filtering, the climate state for 2000 would necessarily include model-simulated ''observed'' data from the last nine years of the twentieth century and the first nine years in the twenty-first century. In that way the ensembles would have been running for 10 years by the time the ''present-day'' year of 2010 was reached such that modeled information about low frequency variability in the years preceding the notional start date of 2010 can be used to evaluate ensemble members' skill prior to 2010.

Thus, the low-pass filtering presents not only a logistical issue for predicting low frequency phenomena, but also an opportunity for evaluating future predictions. That is, decadal outlooks 10 to 20 years in the future could use the simulations started in preceding years in relation to the notional present-day start date to provide information that could be useful in eliminating nonskillful ensemble members and thus improve the predictions running into the future. This is different from numerical weather forecasts in which information is required from the initial point out to at least several days in the future, leaving no time to evaluate different ensemble members to see which ones are more skillful than others. Even for ENSO forecasts the predictive information must be available a couple of months out to a year or so in the future. For decadal predictions, by definition, the predictive information is required a decade or two in the future, which affords more time to evaluate how ensemble members are performing.

To illustrate this point, Fig. 1 shows the first three EOFs of the twentieth-century simulation used as the

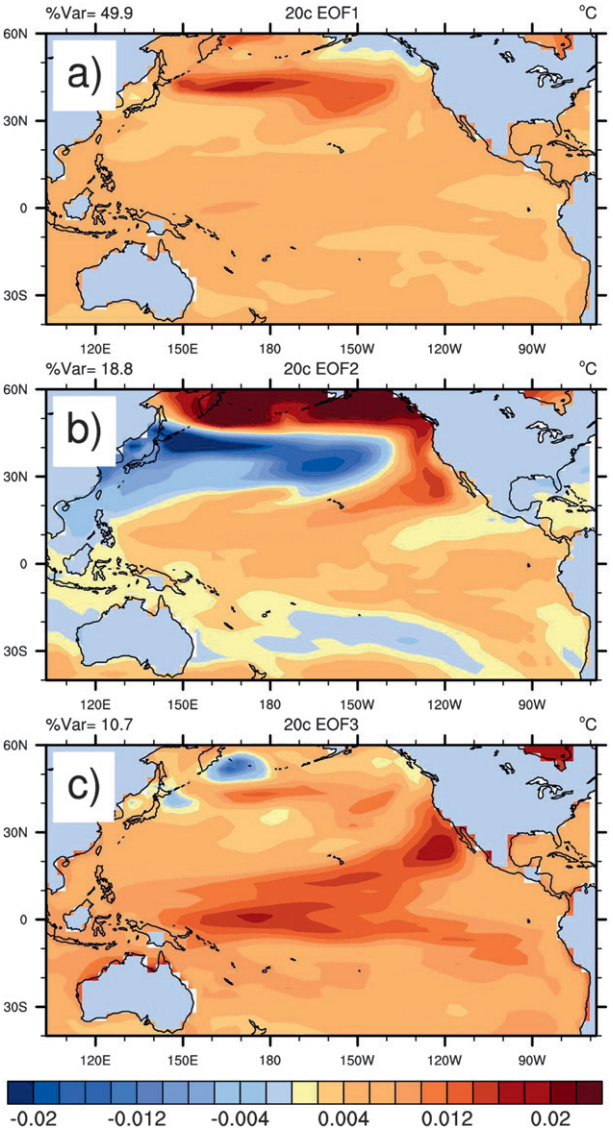

FIG. 1. EOFs of the low-pass filtered SST data from the twentieth-century simulation: (a) EOF1, explaining 49.9% of the variance; (b) EOF2, explaining 18.8% of the variance; and (c) EOF3, explaining 10.7% of the variance.

reference for the start of the large ensemble of future climate simulations (note that the SST stops at 40°S to be consistent with previous analyses of the IPO that included historical observational SST data that are less reliable south of that latitude—e.g., Meehl et al. 2009b). As defined by Meehl et al. (2009b), the first EOF is mostly a trend coming mainly from increasing greenhouse gas forcing and climate change commitment with similar-sign values over the entire basin that explain 49.9% of the low-pass filtered variance. The second EOF has the IPO-type pattern with the tropical Pacific and subtropical northeastern and southeastern Pacific with one sign, and opposite sign regions in the subtropical northwest and southwest parts of the basin explaining 18.8% of the variance. The third EOF has elements of the trend and IPO decadal variability and explains 10.7% of the variance. Thus, the first two EOFs together account for 68.7% of the SST variance, while the first three explain 79.4% of the variance. Excluding EOF3 from the analysis does not substantially change the results, but including it does account for more variance, and that is what we do below.

As noted by Meehl et al. (2009b), the trend and IPO patterns share elements in common, and thus it is difficult to totally separate the two. However, Meehl et al. (2009b) document that interpreting EOF1 as trend and EOF2 as the IPO is a good first-order approximation of the two phenomena.

To track the IPO, EOF2 in Fig. 1b is correlated with the original low-pass filtered Pacific SST data for the twentieth and twenty-first centuries from the ensembles. The time series of pattern correlations is shown in Fig. 2a for the twentieth century (black and green lines), the twenty-first century perfect model reference simulation (blue line), and for nine members of the twenty-first century ensemble chosen subjectively to qualitatively track the time evolution of the IPO. As can be seen in Fig. 2a, although the ensembles branched at the year 2000, owing to the low-pass filtering they begin to actually spread after 1991 as described above (i.e., 1992 represents data from 1983 to 2001 due to the low-pass filtering, and 2001 is one year after the ensembles branched, which introduces a small spread seen already in 1992 and the following years). The spread grows to the year 2000 as at this time the low-pass filtering takes information from the last nine years of the twentieth century and the first nine years of the twenty-first. In any case, these nine ensemble members reflect IPO correlation values near zero in 2005, rising to near +0.6 near 2010 and falling again to about +0.3 in 2020. Recall that the values plotted for 2020 take into account data out to 2029.

However, if the other 20 ensemble members are plotted in a similar way (Fig. 2b), there is much more spread and thus less predictability. The information that went into the plotted values at the year 2000 has already produced considerable spread that only gets larger as the predictions continue into the twenty-first century. Thus, in this subjective evaluation, about 9 members (31%) seem to show some skill in qualitatively following the evolution of the IPO, and 20 do not.

Examination of Fig. 2 suggests that a better prediction of the IPO for the period centered on 2020 would be possible if there was some way of objectively selecting a subset of skillful ensemble members early in the simulations. Of course there is no way of knowing which

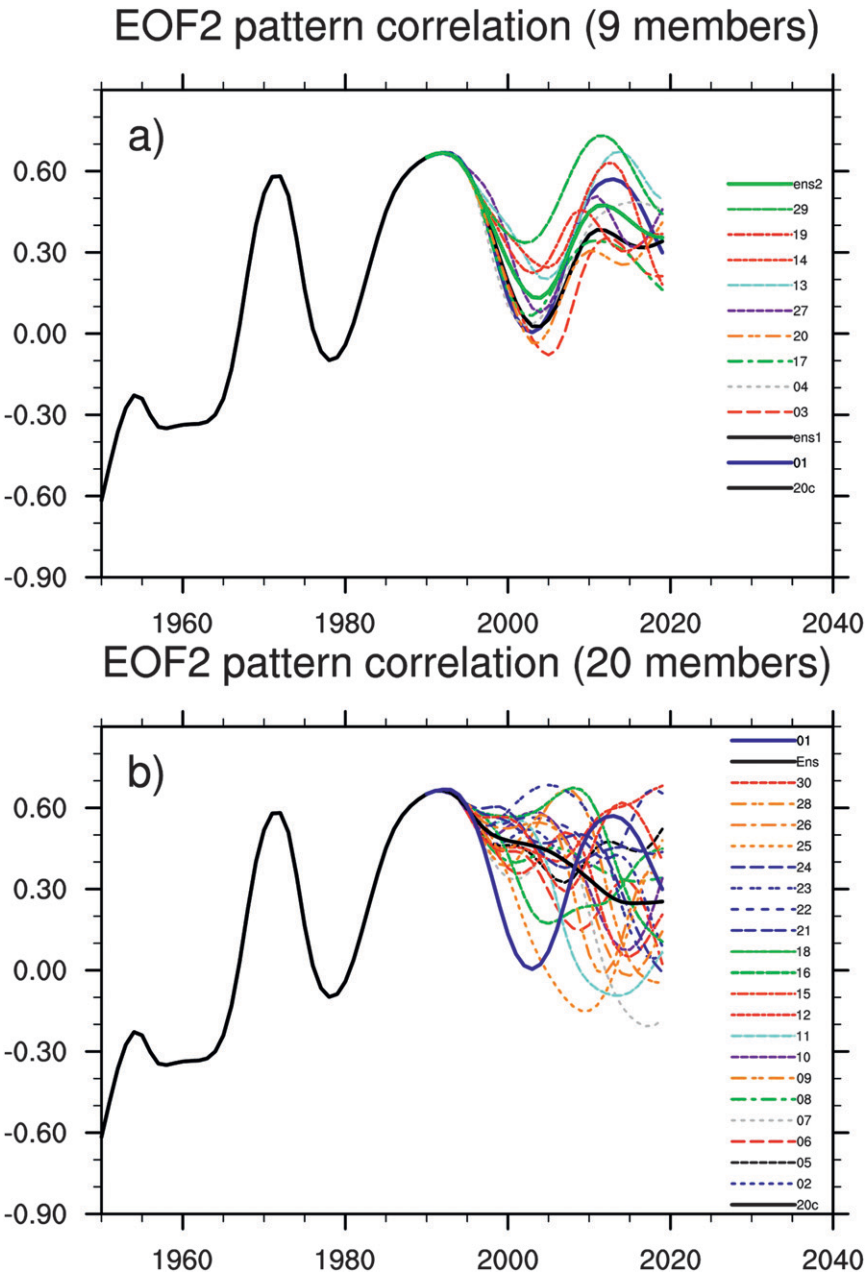

FIG. 2. Pattern correlation of EOF2 from Fig. 1b with original low-pass filtered SST data for the twentieth and twenty-first centuries: (a) subjectively chosen nine "best" ensemble members that track the reference perfect model simulation (blue line) and the ensemble average of these nine members (green line) and (b) as in (a) but for the remaining 20 ensemble members; ensemble average is the black line.

members will perform better when the ensembles branch in 2000. However, in the first 9 years there is considerable divergence in about 70% of the ensemble members (thus producing the spread for the data plotted for the year 2000 that takes into account the previous and following 9 years in the low-pass filtering). If the decadal prediction is for time periods at least 10 years in the future in relation to the notional start date of 2010, that means for simulations started in 2000, by 2010 there are observations covering the entire period centered on 2000, and the spread of the ensemble members could be evaluated at that time and a subset selected. This is because, as seen in Fig. 2a, a number of ensemble members that are successful in tracking the IPO in 2000 continue to do so out to 2020.

This method of subselecting more skillful ensemble members has been attempted in other prediction contexts, for example, a method called ''dynamic stratification'' for numerical weather prediction (Schubert et al. 1992). However, since the evaluation time is short for a six-day forecast, dynamic stratification relies on making a statistical evaluation of more skillful initial states. For the decadal prediction problem, the first decade of a simulation prior to the present-day start date can be used to subselect more skillful ensemble members to improve the skill of the predictions over the years following that notional start date.

Therefore, the decadal prediction methodology used in this paper can be summarized as follows:

1) Low-pass filter all model data (center year represents about a 19-yr average).
2) Using Pacific SSTs, calculate EOFs for the twentieth century, first removing the twentieth-century annual mean.
3) Compute PC time series for first three EOFs.
4) Regress principal component (PC) time series from first three EOFs against original SST data and sum to reconstruct patterns of time-evolving SST for twentieth century; then compare these reconstructed patterns to actual patterns to quantify how well past SSTs can be characterized with the reconstructions since this method will be used for the future SST predictions.
5) Calculate predicted PC time series using twentieth-century EOFs projected on to future predicted SSTs for each ensemble member (the same twentieth-century mean is removed).
6) Correlate the second EOF pattern with the low-pass filtered data for each ensemble member and calculate the Euclidean distance from each ensemble member from the reference case in the 10-yr period from 1991–2000; the ensemble members with the lowest summed distance are chosen.
7) Use the selected subset PC time series predictions and the pattern of each twentieth-century EOF to produce future SST anomaly patterns; then sum the first three to get total contribution of first three EOFs and average those results across the subset ensemble members to get the SST anomaly patterns for each year as a prediction.
8) Correlate those patterns with target SST anomalies as prediction verification at various future time periods.

4. Decadal predictions of Pacific SSTs

Using the first three EOFs of twentieth-century climate from the reference model simulation as a starting point (Fig. 1), the PC time series from these EOFs are regressed against the original data and the patterns are summed to reconstruct Pacific SST anomaly patterns during the twentieth century. This serves as a check for what could be expected for the twenty-first century predictions. Figure 3 shows the (left) reference and (right) reconstructed SST anomalies for every five years starting in 1960. Recall that the year is centered on the 19-yr time period due to the low-pass filtering. The reconstructed SST anomaly patterns qualitatively resemble the reference ones, including the tropical Pacific cooling in the period centered on 1965. Pattern correlations between the reconstructed and reference SSTs (at upper right of right-hand panels) range from +0.44 (1970) to +0.84 (1980). In general, the reconstructed SST patterns have lower amplitude than the reference, partly because, as noted above, only the first three EOFs are used for the reconstructions. The plots in Fig. 3 represent a kind of running average representation of the target and reconstructed SSTs for the twentieth century and are not meant to quantify statistical significance.

As discussed earlier, the second EOF or IPO pattern is postulated as an important possible source of regional predictive skill, so the subsetting of the ensemble members is done using the second EOF that represents the IPO. Therefore, the second EOF pattern in Fig. 1b is correlated with the low-pass filtered data for each ensemble member and then the subset of ensemble members is chosen that best captures the IPO (or EOF2) evolution by calculating the Euclidean distance from each ensemble member from the reference case in the 10-yr period from 1991 to 2000. The distances are summed and the ensemble members with the lowest summed distance are chosen. As could be expected from Fig. 2a, this number is likely to be less than 10 and, indeed, the best seven to nine ensemble members produce about the same level of skill by this measure. Therefore, we choose the larger number, nine ensemble members, and the ''most skillful'' are illustrated in Fig. 4 where the time evolution of the EOF2 pattern correlations (as in Fig. 2a) are plotted for the nine-member subset (ensemble average is red solid line; range is given by red hatching) compared to the other 20 ensemble members (ensemble average is solid blue line; range is blue hatching). The ensemble average of the nine more skillful members better follows the reference case (black line) compared to the other ensemble members, with a summed range that is smaller than the less skillful ensemble members.

Although we have structured the methodology to predict the future time evolution of the unperturbed reference simulation, it could also be possible to use each of the other 29 members as the reference case, apply the same methodology to choose the most skillful subset, and track how they predict the future evolution of EOF2. The three lower panels in Fig. 4 show three measures of

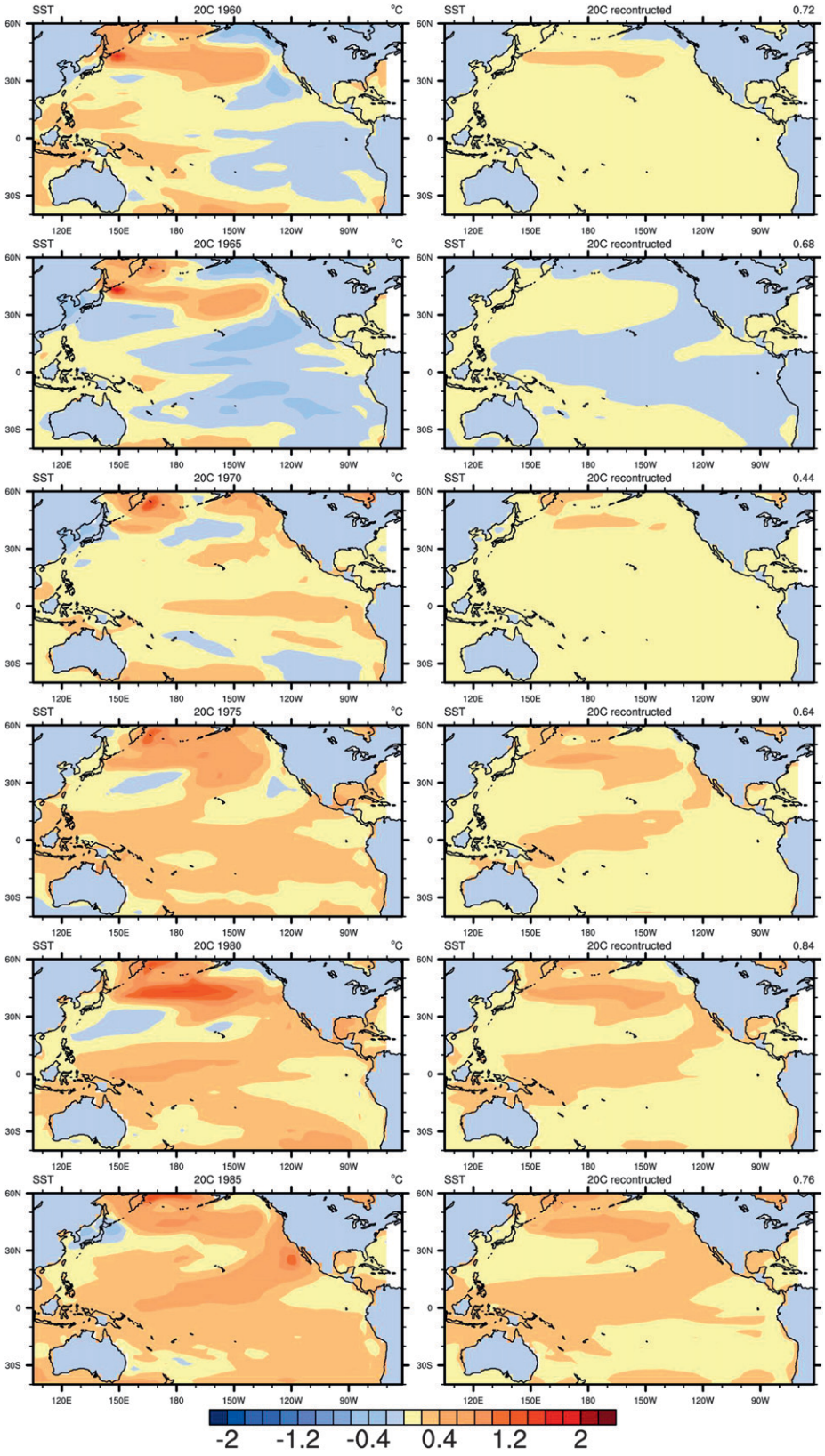

FIG. 3. (left) Original low-pass filtered SST anomalies, plotted every five years as indicated in the panel labels from (top) 1960 to (bottom) 1985. (right) As in the left panels but for reconstructed SST anomalies from the first three EOFs. The year indicated actually represents a 19-yr period centered on that year.

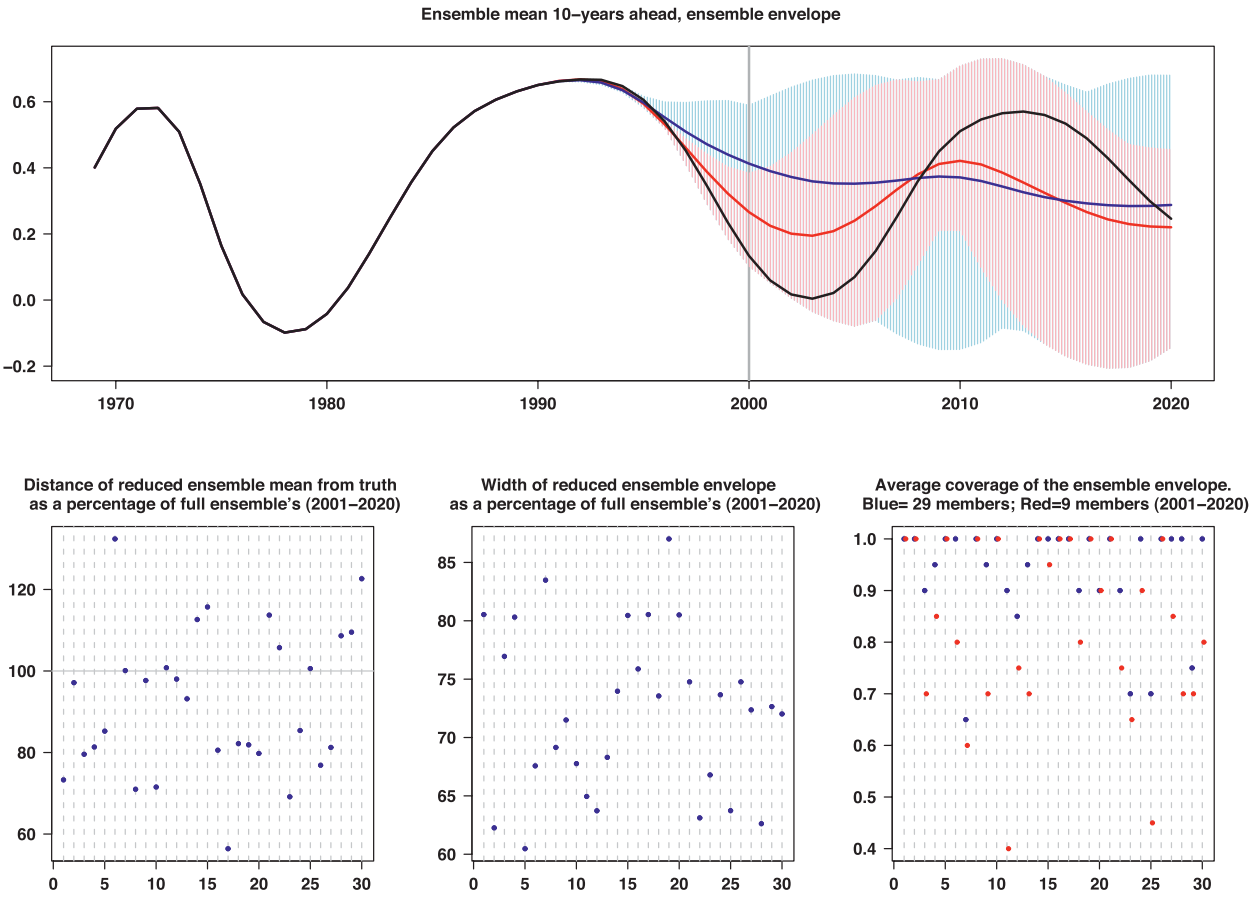

FIG. 4. (top) Reference time series of pattern correlations for EOF2, in black (as in Fig. 1a); the blue line is the ensemble mean from the full set of members (29), light blue shading is the full ensemble spread, the red line is the reduced ensemble mean (nine members objectively chosen as explained in section 3), and the pink shading is the reduced ensemble spread. (bottom) From left to right, three measures of performance (accuracy, precision, and coverage) are evaluated using each of the 30 ensemble members as a reference. See section 4 for details.

forecast performance evaluated over all 30 cases (by using each ensemble member as a reference, numbered from 1 to 30 on the *x* axis). The first measure is chosen as the Euclidean distance of the ensemble mean prediction, and the lower left panel shows what percentage of the full ensemble mean prediction distance is represented by the reduced ensemble mean prediction distance. Thus, the most skillful nine ensemble members are chosen for each reference simulation as above; the Euclidean distance between the reference case and the reduced ensemble mean, after 2001, is divided by the Euclidean distance from the full ensemble mean; and the ratio (multiplied by 100) is plotted on the *y* axis. A ratio of less than 100 shows that the prediction produced by the subset of ensemble members is more skillful than the full ensemble. Out of the 30 possible reference predictions, 10 are less skillful than the full ensemble for predicting the IPO in the future out to 2020. Thus, in two-thirds of the cases, the subset ensemble is more skillful by this measure.

Another measure of performance for an ensemble of simulations is the precision of the forecast, which can be measured in terms of the spread of the ensemble. This result is shown in the lower middle panel in Fig. 4 where the range of the reduced ensemble (R1, defined as the sum of the ranges at each time point between 2010 and 2020) is divided by the range of the full ensemble (R0). The lower this ratio, the better the skill of the reduced ensemble. Note that all 30 values of the ratio (R1/R0 × 100, by definition less than or equal to 100) lie well below 100, and about two-thirds are below 75, with seven below 65, indicative of enhanced skill. Finally, in the lower right panel of Fig. 4, a measure of coverage (defined as the fraction of times in the forecast period when the reference case lies within the range of either the reduced or full ensemble) is plotted for each of the 30 test cases. A value of 1.0 means the reference case is always captured by the spread of the ensemble. There are two dots for each case, one for the full ensemble (blue) and one

for the reduced ensemble (red). There are only 17 out of 30 cases when the full ensemble spread captures the reference case at each point in time. Of these cases, 11 are also captured perfectly by the reduced ensemble spread. There are only four cases for which the reduced ensemble coverage falls below 70% (and of these, three are cases when also the full ensemble coverage is at 70% or below), indicating that the reduced ensemble members do a reasonable job of at least capturing the envelope of the actual evolution of the IPO in future climate.

The three twentieth-century EOFs are next regressed on to the subset of nine more skillful future ensemble members that were selected in Fig. 4a, and the corresponding PC time series are calculated and shown in Fig. 5. It can be seen that the forced trend (EOF1) has the least spread of future PC time series (Fig. 5a), while EOF3 has the greatest spread (Fig. 5c). The IPO (EOF2, Fig. 5b) reflects the qualitative tracking of the reference case out to 2020 as illustrated by Fig. 4.

Following the lines in these plots out to 2030 shows similar results for EOF1 and EOF3, with the large trend dominating the time evolution. For EOF2, any skill captured in the first 20 years dissipates after 2020 with an almost random spread of the ensemble members (Fig. 5). This indicates the increasing dominance of the forced trend the longer the simulations are run into the future.

These future PC time series are then regressed onto the EOFs in Fig. 1 and averaged across the subset ensemble members. Figure 6 shows how the three EOFs contribute to the reference SST anomaly patterns for the prediction in 2020. The trend EOF1 (Fig. 6b) clearly has a large contribution to the overall warming in the Pacific (Fig. 6a) with an anomaly pattern correlation of +0.60. However, the IPO pattern in Fig. 6c has a pattern correlation of +0.27, while EOF3 in Fig. 6d has the lowest contribution with a pattern correlation of near zero.

To contrast the reconstructed contributions to the reference simulation for 2020 in Fig. 6 to those in 2010, the IPO (EOF2) actually has a larger contribution (pattern correlation of +0.54) compared to the trend EOF1 (pattern correlation of +0.47) (not shown). Thus, the passage of a decade (from 2010 to 2020) shows that the growing external forcing from increasing GHGs begins to overwhelm the contributions from the IPO.

The regression patterns are then summed to construct the total predicted SST anomaly patterns for the future. These patterns are compared to the reference case in Fig. 7, with the reference case SST anomalies on the left and the reconstructed predictions from the first three EOFs on the right. There is an anomaly pattern correlation of +0.63 for the period centered on 2010 (Fig. 7b) and +0.67 for the prediction period centered on the year 2020. As in the twentieth-century reconstructions in Fig. 3, the future reconstruction (Fig. 7d) shows a lower amplitude SST anomaly pattern than the reference (Fig. 7c), again partly as a result of using just the first three EOFs, although the major features of the future SST evolution are predicted

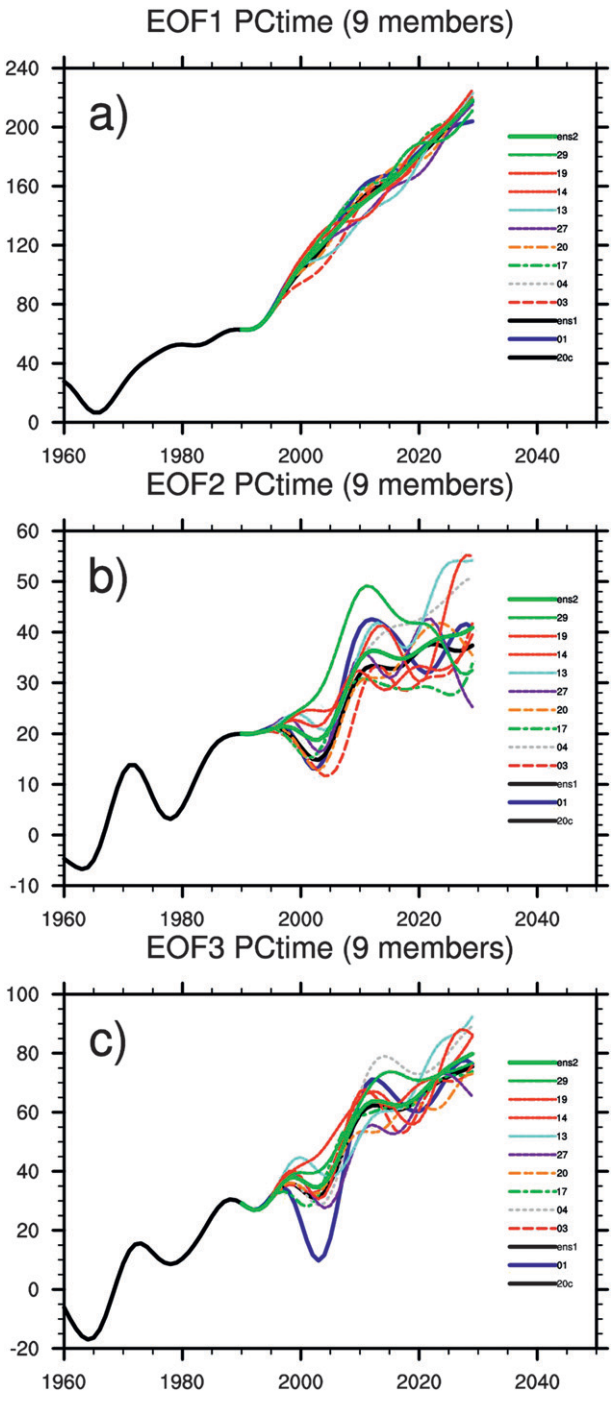

FIG. 5. Principal component time series formed by regressing the three twentieth-century EOFs (Fig. 1) onto the selected nine future ensemble members for (a) EOF1, (b) EOF2, and (c) EOF3. The reference member is the blue line.

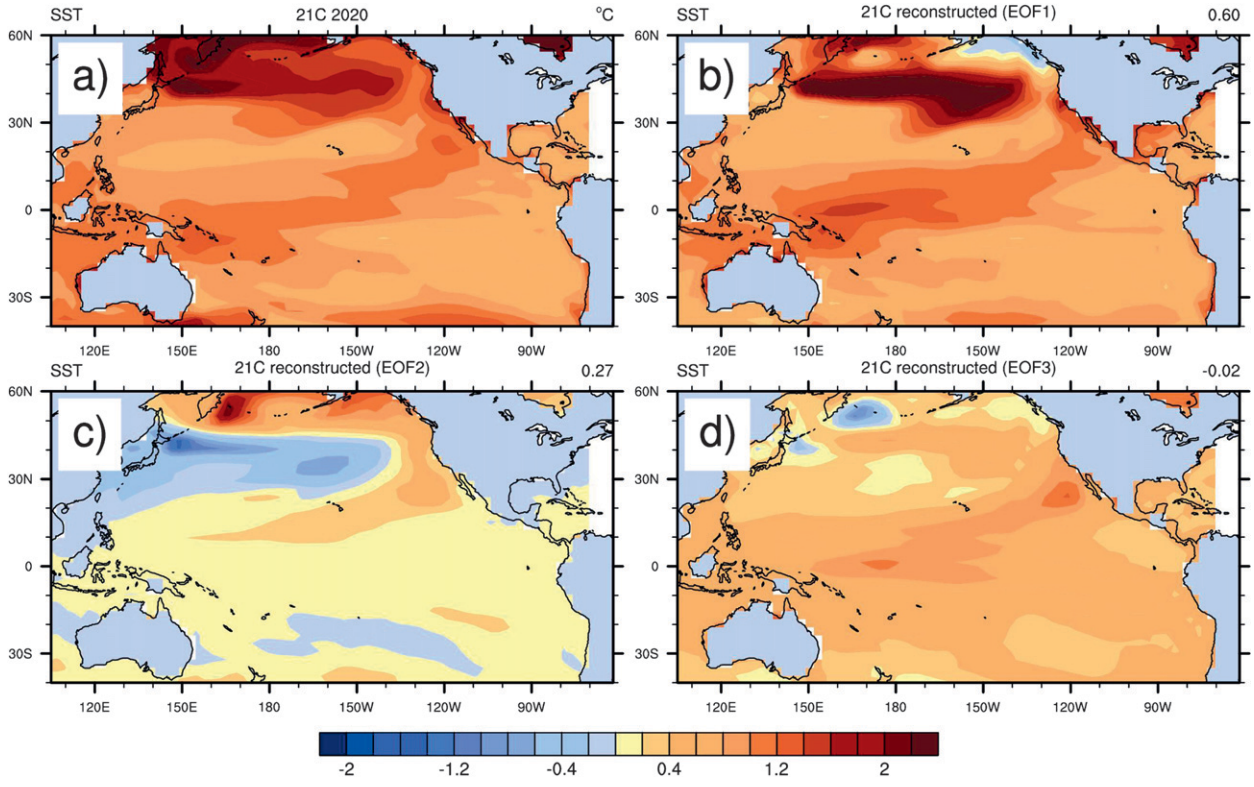

FIG. 6. (a) Reference simulation SST anomalies for the 19-yr period centered on 2020. (b) Contribution of predicted EOF1 to predicted SSTs in 2020. (c) As in (b) but for EOF2. (d) As in (b), but for EOF3.

for 2020 by the reduced ensemble. The anomaly pattern correlation for the 19-yr prediction centered on 2030 is less than for 2020, with a value of +0.59 (not shown).

As a check to see how well the reduced ensemble is performing compared to what could be expected from the full ensemble, Fig. 8 shows the time evolution of the pattern correlations for the reconstructed SST anomaly patterns with the reference case for the reduced ensemble (Fig. 8a) and the other 20 ensemble members (Fig. 8b). For the year 2015, the spread in the reduced ensemble is 0.08 while it is 0.15 in the rest of the ensemble, while for 2020 the spread in the reduced ensemble is 0.03, and for the rest of the ensemble members the spread is 0.08. Thus, using the reduced ensemble results in a reduction of about half the ensemble prediction spread over and above the remaining ensemble members. To test the significance of this result, for the year 2020, random sets of nine values are drawn from the full 30-member ensemble, and for each set of nine values the range is compiled as the lowest to highest value of the nine members. All combinations are formed into a probability density function that indicates the chance for a range smaller than the value of 0.03 for the nine-member selected set is 2.6%, so the smaller range for the reduced ensemble is significant at the 97.4% level.

5. An application to North American and Australian precipitation

Although Pacific SSTs are of interest because of some knowledge we may have of mechanisms that could produce predictability over that region, it is also of interest to attempt to estimate quantities of relevance to stakeholders in regions where climate has been shown to be influenced by low frequency variability of Pacific SSTs such as North America and Australia (e.g., Meehl and Hu 2006). As noted earlier, there are processes associated with decadal variability in the Atlantic, such as the AMO, that also have been shown to influence North American precipitation. However, for the present application we focus on the contribution from the Pacific SSTs, mindful that taking into account additional decadal SST variability in the Atlantic could increase predictive skill over North America. Additionally there are influences from South Asia that could affect Australian precipitation as well as Pacific SSTs.

Using a similar methodology for reconstructing the future SST anomaly patterns in Fig. 7, we calculate a precipitation outlook for the 19 years centered on 2020 in Fig. 9 for North America and Fig. 10 for Australia. We use the predicted reduced ensemble PC time series from the SST

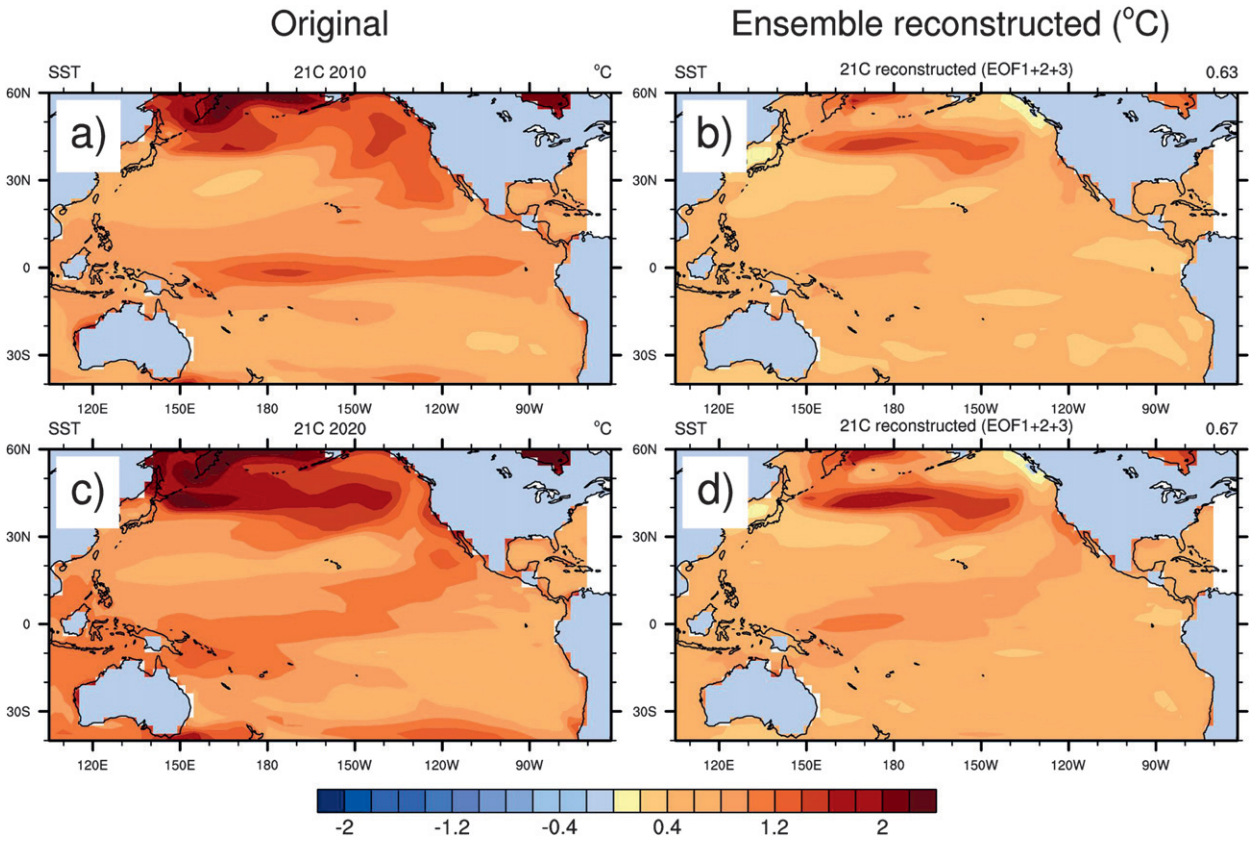

FIG. 7. Reference simulation SST anomalies for 19-yr periods centered on (a) 2010 and (c) 2020. Regression patterns for the first three EOFs summed to construct the predicted SST anomaly patterns for 19-yr periods centered on (b) 2010 and (d) 2020.

EOFs, regress them onto the low-pass filtered precipitation data, and sum those patterns to produce predicted precipitation anomalies. First, for North America the predicted pattern for the 19-yr period centered on 2020 in Fig. 9b is compared to the reference pattern in Fig. 9a. The major features in the reference case (Fig. 9a) of increased precipitation in northern North America and the Mississippi basin with reduced precipitation over the southwest and eastern United States are reproduced in the prediction for the period centered on 2020 with an anomaly pattern correlation of +0.38 (Fig. 9b).

The same procedure is followed to produce patterns of predicted precipitation over Australia for the 19-yr period centered on 2020 (Fig. 10b) compared to the reference case (Fig. 10a). As with the North American result in Fig. 9, the pattern of predicted precipitation over Australia qualitatively captures the reference case. There is above-normal precipitation predicted over New South Wales and extending to northern Australia and below-normal precipitation for southern Victoria and central Australia (Fig. 9) with an anomaly pattern correlation of +0.61. This greater skill compared to North America (+0.38) could reflect the stronger connection of Australian rainfall to Pacific SSTs in general and the IPO in particular (Arblaster et al. 2002).

6. Conclusions

Decadal prediction of Pacific SSTs is addressed in a perfect model experiment where an unperturbed reference simulation of twentieth- and twenty-first-century climate (the latter following the A1B scenario) is predicted by a perturbed 29-member ensemble (the perturbations occurring only in the atmosphere). This can be considered a conservative example since the initial ocean and sea ice state is perfectly known and the predictions have only small perturbations in the atmosphere from starting the model on different days near 1 January 2000.

There are two guiding principles for the methodology that concentrates only on the low frequency part of the climate system (all data are low-pass filtered). First, it is assumed that much of the predictability can be captured by the first three EOFs for which EOF1 is interpreted to be mostly the climate change commitment and forced trend, EOF2 resembles a dominant mode of decadal climate

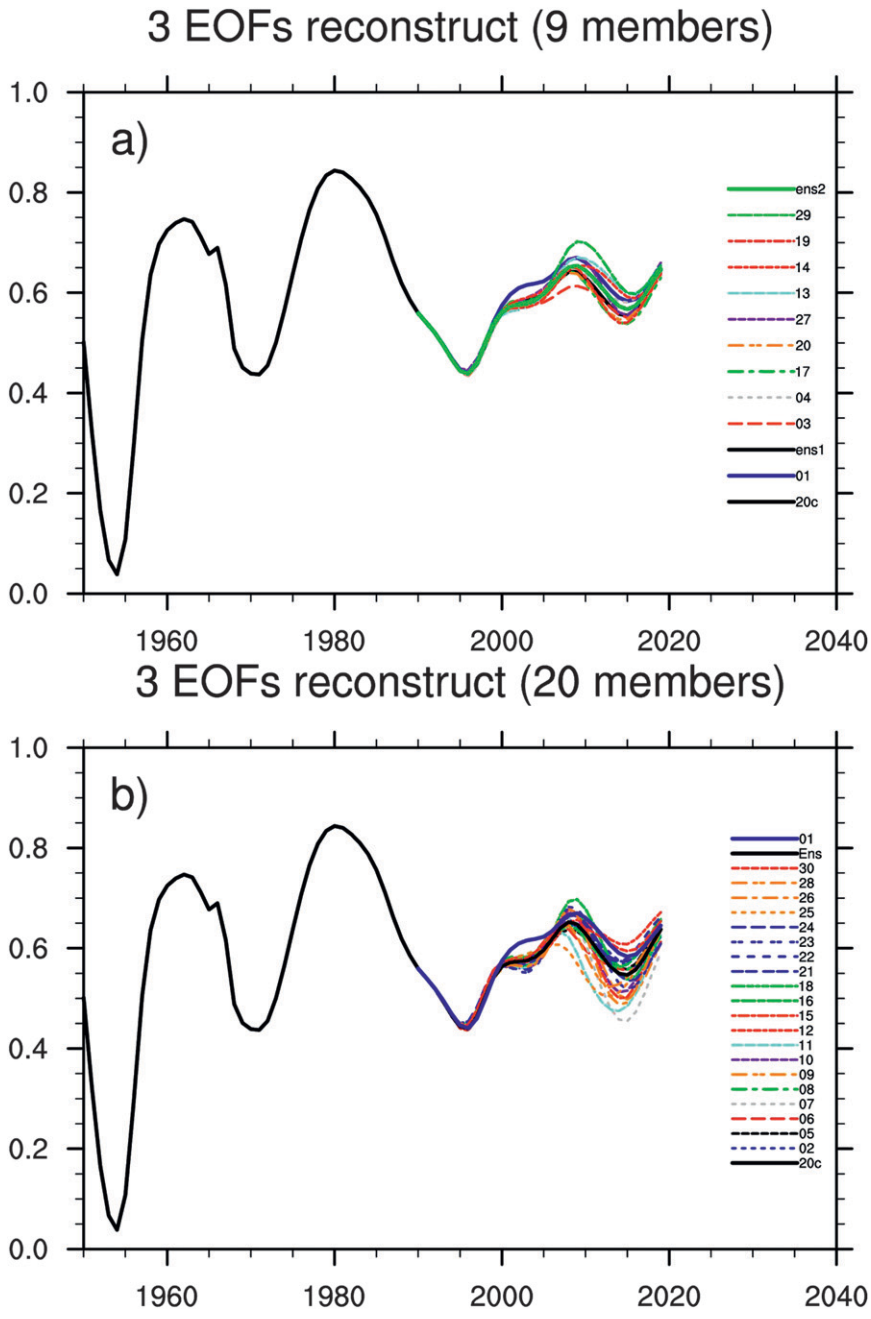

FIG. 8. Time evolution of the pattern correlation for the reconstructed SST anomaly patterns with the reference simulation for (a) the 9-member reduced ensemble and (b) the other 20 ensemble members. The reference simulation is shown by the blue line.

variability in the Pacific called the interdecadal Pacific oscillation (a Pacific basin version of the Pacific decadal oscillation, defined only for the North Pacific), and EOF3 contains elements of the first two. Nearly 80% of the twentieth-century low-pass filtered SST variance is captured by these three EOFs. The second guiding principle is that decadal variations of the IPO (EOF2) may provide some increase in regional prediction skill over and above the forced trend and climate change commitment, and for the IPO there will be a more skillful subset of ensemble members that can be identified early in the prediction period that will continue to track the evolution of EOF2 into the future more skillfully than the rest of the ensemble members.

A method of selecting a more skillful subset relies on the concept that modeled information about low frequency

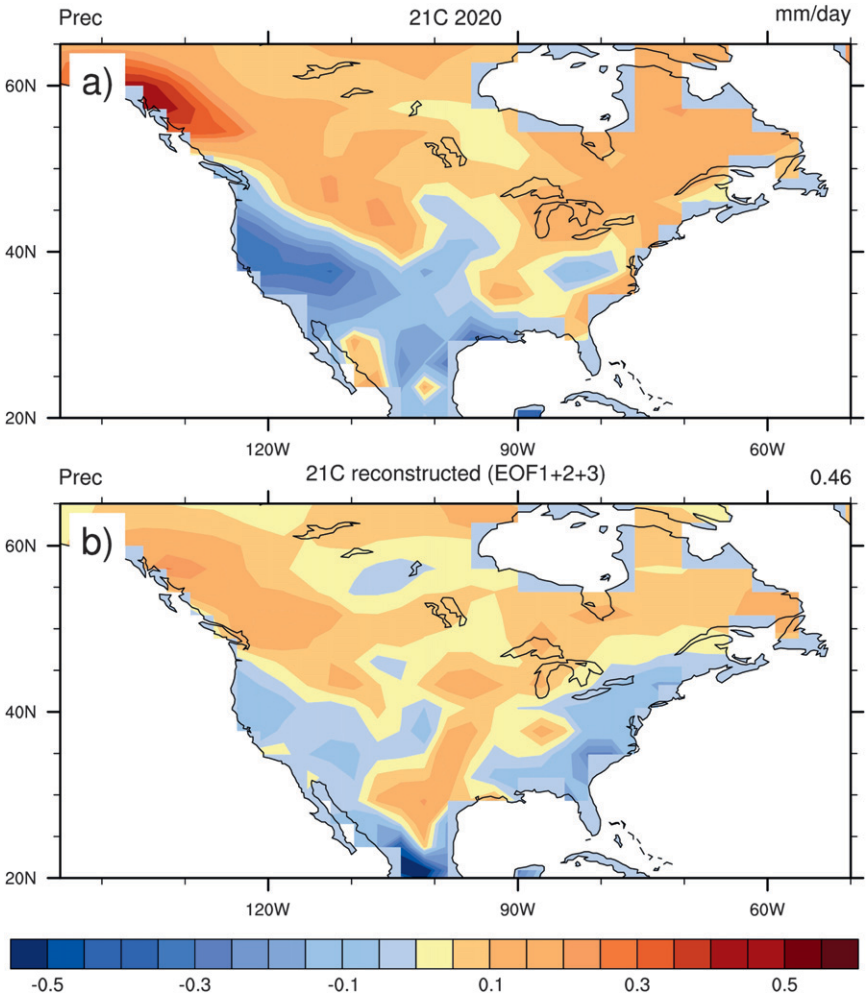

FIG. 9. North American precipitation anomalies for the 19-yr period centered on 2020 computed by regressing the reduced ensemble PC time series from the three SST EOFs in Fig. 5 onto the low-pass filtered precipitation data: (a) reference simulation and (b) predicted.

variability from years preceding the notional start date can be used to evaluate and eliminate less skillful ensemble members. The selected subset of ensemble members can then be applied to the 10 to 20 years of the prediction after that notional start date. For this exercise it is assumed that this start date is the year 2010, and ensemble members branched from an initial state in the year 2000. Thus, by 2010 there are already 10 years of observations that can be used to reject nonskillful ensemble members. This number amounts to less than 10 using a measure of summed spread from the reference case (nine are used here). This subset is then used to compute future PC time series that are projected back onto the original three EOFs of Pacific SSTs. The results are summed and averaged over the subset ensemble to construct predictions past 2010 that can be evaluated with respect to the reference case. The anomaly pattern correlation for the outlook for the 19 years centered on 2020 for Pacific SSTs is +0.67 in this case and +0.59 for 2030.

An application of the predicted SSTs in the Pacific is made to North American and Australian precipitation. Using the same future PC time series derived from the Pacific SSTs projected on the low-pass filtered North American and Australian precipitation data shows that the prediction of the 2020 period qualitatively captures the regional aspects of precipitation changes for that time period. For North America there are increases over the north-central states and Midwest with decreases over the southwest and eastern United States, with an anomaly pattern correlation of +0.38. Over Australia for the 2020 period, above-normal precipitation is predicted for much of New South Wales and extending to northern Australia and below-normal precipitation for southern Victoria and central Australia, with an anomaly pattern correlation

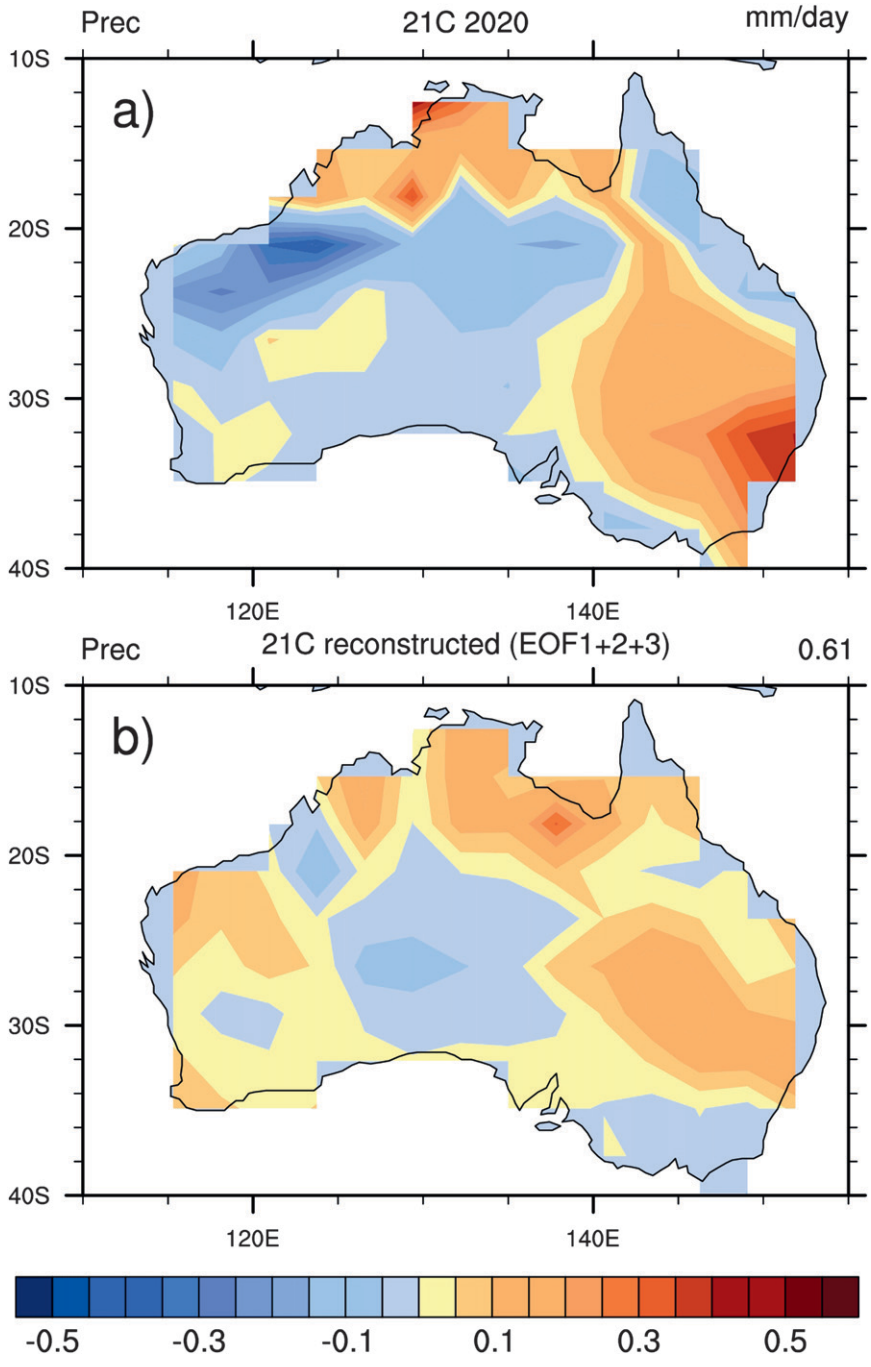

FIG. 10. As in Fig. 9 but for Australian precipitation anomalies.

of +0.61. The greater skill for the predicted pattern of Australian rainfall compared to North American precipitation could reflect the stronger connection of Australian rainfall to Pacific SSTs.

For 2010 (the end of the ensemble evaluation period), the Pacific SST ensemble members have a higher contribution from the IPO compared to the forced trend, but by 2020 the forced trend is dominant. Predictions beyond 2020 indicate that almost all of the signal is from the forced trend. This suggests that by 2020 the IPO is already becoming swamped by the forced trend, and any regional skill from the IPO would have been overwhelmed by the forcing. Thus, one could ask what the results would look like if a simple full ensemble average were used for a prediction of SST anomalies over the Pacific basin and precipitation anomalies over North

America and Australia rather than the reduced ensemble. Results show that by 2020 and on to 2030, the influence from the IPO is dominated by the forced trend since the anomaly pattern correlations for SST reconstructed from projecting the PC time series for the first three EOFs derived from the full 29-member ensemble compared to the 9-member reduced ensemble are similar. Thus, these results indicate that in an era of rapidly increasing forcing from increasing GHGs, most regional predictive skill at time periods longer than a decade arises from the forced trend, with lesser contributions from the IPO.

Acknowledgments. Portions of this study were supported by the Office of Science (BER), U.S. Department of Energy, Cooperative Agreement DE-FC02-97ER62402, and the National Science Foundation.

REFERENCES

Arblaster, J. M., G. A. Meehl, and A. Moore, 2002: Interdecadal modulation of Australian rainfall. *Climate Dyn.,* **18,** 519–531.

Boer, G. J., 2010: Decadal potential predictability of twenty-first century climate. *Climate Dyn.,* in press.

Collins, W. D., and Coauthors, 2006: The Community Climate System Model version 3 (CCSM3). *J. Climate,* **19,** 2122–2143.

Deser, C., A. S. Phillips, and J. W. Hurrell, 2004: Pacific interdecadal climate variability: Linkages between the tropics and the North Pacific during boreal winter since 1900. *J. Climate,* **17,** 3109–3124.

Enfield, D. B., A. M. Mestas-Nuñez, and P. J. Trimble, 2001: The Atlantic Multidecadal Oscillation and its relation to rainfall and river flows in the continental U.S. *Geophys. Res. Lett.,* **28,** 2077–2080.

Folland, C. K., D. E. Parker, A. Colman, and R. Washington, 1999: Large-scale modes of ocean surface temperature since the late nineteenth century. *Beyond El Niño: Decadal and Interdecadal Climate Variability.* A. Navarra, Ed., Springer-Verlag, 73–102.

Hawkins, E., and R. Sutton, 2009: The potential to narrow uncertainty in regional climate predictions. *Bull. Amer. Meteor. Soc.,* **90,** 1095–1107.

Hurrell, J., G. A. Meehl, D. Bader, T. Delworth, B. Kirtman, and B. Wielicki, 2009: A unified modeling approach to climate system prediction. *Bull. Amer. Meteor. Soc.,* **90,** 1819–1832.

Karoly, D. J., and Q. Wu, 2005: Detection of regional surface temperature trends. *J. Climate,* **18,** 4337–4343.

Keenlyside, N., M. Latif, J. Jungclaus, L. Kornblueh, and E. Roeckner, 2008: Advancing decadal-scale climate prediction in the North Atlantic sector. *Nature,* **453,** 84–88.

Kirtman, B. P., and D. Min, 2009: Multimodel ensemble ENSO prediction with CCSM and CFS. *Mon. Wea. Rev.,* **137,** 2908–2930.

——, J. Shukla, M. Balmaseda, N. Graham, C. Penland, Y. Xue, and S. Zebiak, cited 2002: Current status of ENSO forecast skill. A report to the Climate Variability and Predictability (CLIVAR) Numerical Experimentation Group (NEG), CLIVAR Working Group on Seasonal to Interannual Prediction. [Available online at http://www.clivar.org/publications/wg_reports/wgsip/nino3/report.htm.]

Knight, J., R. J. Allan, C. K. Folland, M. Vellinga, and M. E. Mann, 2005: A signature of persistent natural thermohaline circulation cycles in observed climate. *Geophys. Res. Lett.,* **32,** L20708, doi:10.1029/2005GL024233.

Lee, T. C. K., F. W. Zwiers, X. Zhang, and M. Tsao, 2006: Evidence of decadal climate prediction skill resulting from changes in anthropogenic forcing. *J. Climate,* **19,** 5305–5318.

Meehl, G. A., and A. Hu, 2006: Megadroughts in the Indian monsoon region and southwest North America and a mechanism for associated multi-decadal Pacific sea surface temperature anomalies. *J. Climate,* **19,** 1605–1623.

——, W. M. Washington, W. D. Collins, J. M. Arblaster, A. Hu, L. E. Buja, W. G. Strand, and H. Teng, 2005: How much more global warming and sea level rise? *Science,* **307,** 1769–1772.

——, and Coauthors, 2006: Climate change projections for the twenty-first century and climate change commitment in the CCSM3. *J. Climate,* **19,** 2597–2616.

——, and Coauthors, 2007: Global climate projections. *Climate Change 2007: The Physical Science Basis.* S. Solomon et al., Eds., Cambridge University Press, 747–845.

——, and Coauthors, 2009a: Decadal prediction: Can it be skillful? *Bull. Amer. Meteor. Soc.,* **90,** 1467–1485.

——, A. Hu, and B. D. Santer, 2009b: The mid-1970s climate shift in the Pacific and the relative roles of forced versus inherent decadal variability. *J. Climate,* **22,** 780–792.

Mochizuki, T., and Coauthors, 2010: Pacific decadal oscillation hindcasts relevant to near-term climate prediction. *Proc. Natl. Acad. Sci. USA,* **107,** 1833–1837.

Parker, D. E., C. K. Folland, A. A. Scaife, J. Knight, A. Colman, P. Baines, and B. Dong, 2007: Decadal to multidecadal variability and the climate change background. *J. Geophys. Res.,* **112,** D18115, doi:10.1029/2007JD008411.

Pohlmann, H., J. H. Jungclaus, A. Köhl, D. Stammer, and J. Marotzke, 2009: Initializing decadal climate predictions with the GECCO Oceanic Synthesis: Effects on the North Atlantic. *J. Climate,* **22,** 3926–3938.

Power, S., T. Casey, C. Folland, A. Colman, and V. Mehta, 1999: Inter-decadal modulation of the impact of ENSO on Australia. *Climate Dyn.,* **15,** 319–324.

Schubert, S., M. Suarez, J.-K. Schemm, and E. Epstein, 1992: Dynamically stratified Monte Carlo forecasting. *Mon. Wea. Rev.,* **120,** 1077–1088.

——, and Coauthors, 2009: A U.S. CLIVAR project to assess and compare the responses of global climate models to drought-related SST forcing patterns: Overview and results. *J. Climate,* **22,** 5251–5272.

Smith, D., S. Cusack, A. Colman, C. Folland, G. Harris, and J. Murphy, 2007: Improved surface temperature prediction for the coming decade from a global climate model. *Science,* **317,** 796–799.

Sutton, R. T., and D. L. R. Hodson, 2005: Atlantic Ocean forcing of North American and European summer climate. *Science,* **309,** 115–118.

Tang, Y., Z. Deng, X. Zhou, Y. Cheng, and D. Chen, 2008: Interdecadal variation of ENSO predictability in multiple models. *J. Climate,* **21,** 4811–4833.

Teng, H., and G. Branstator, 2010: Initial-value predictability of prominent modes of North Pacific subsurface temperature in a CGCM. *Climate Dyn.,* in press.

Timmermann, A., and Coauthors, 2007: The influence of a weakening of the Atlantic meridional overturning circulation on ENSO. *J. Climate,* **20,** 4899–4919.

Xie, S.-P., C. Deser, G. A. Vecchi, J. Ma, H. Teng, and A. T. Wittenberg, 2010: Global warming pattern formation: Sea surface temperature and rainfall. *J. Climate,* **23,** 966–986.